Two-scale approach to predict multi-site cracking potential in 3-D structures using the generalized finite element method

Francisco Evangelista Jr. [a,*], Jeffery R. Roesler [b], Carlos A. Duarte [b]

[a] Department of Civil Engineering, California State University, Los Angeles, 5151 State University Drive, Los Angeles, CA 90032, USA
[b] Department of Civil and Environmental Engineering, University of Illinois at Urbana-Champaign, 205 North Mathews Avenue, Urbana, IL 61801, USA

ARTICLE INFO

ABSTRACT

This research utilized the novel computational framework of the generalized finite element method (GFEM) to predict the potential for crack propagation in concrete slabs. A two-scale approach, using the global–local concept within the GFEM framework (GFEM^{g-l}), is applied to multi-site cracking problems (MSC), where different crack geometries are placed simultaneously at different positions in a three-dimensional airfield slab loaded by new generation aircraft gears. The GFEM^{g-l} approach efficiently simulated multiple cracks without discretization in the global mesh, but only in the local domain. The GFEM^{g-l} enrichment functions allow the displacements of the local problem to be represented in the global domain through enrichment functions from the local problems rather than explicitly modeling each crack discretely in the global domain. The main contribution of this work was extension of the GFEM^{g-l} approach to a class of three-dimensional MSC problems involving realistic boundaries conditions and existence of multiple cracks spanning different orders of magnitude in size (scales) within the domain. For the linear elastic structure, bottom- and surface-initiated cracks with small dimensions were considered in conjunction with a larger macro-crack. Unlike traditional numerical methods, the proposed GFEM^{g-l} made it possible to tackle this class of problems by avoiding refined crack front meshes in the global domain as well as numerical round-off errors. Furthermore, the two-scale approach significantly reduces the computational cost for large-scale 3-D MSC problems.

© 2013 Elsevier Ltd. All rights reserved.

1. Introduction

An advanced modeling technique that balances accuracy with computational time is required for the class of problems involving cracks with different scale, like in the case of macro-cracks interacting with many meso-cracks. For these cases, the global mesh is generally designed to model the macro-crack and cannot capture the response for meso-cracks. The finite element method (FEM) requires extreme local refinements around the front of macro-cracks and also in regions where meso-cracks are located, leading to a high computational cost, especially in three-dimensional cases (Kim et al., 2008, 2010). An alternative approach to analyze this class of problems is the global–local or sub-modeling procedures implemented in the finite element model (Noor, 1986; Diamantoudis and Labeas, 2005). However, this approach is known to be sensitive to the quality of boundary conditions used in the local domains (sub-models). Several other two- or multi-scale approaches for the analysis of fracture mechanics problems have been proposed recently (Guidault et al., 2008; Loehnert and Belytschko, 2007; McVeigh et al., 2006; Liu and McVeigh, 2008; Ghosh

et al., 2001; Fish, 1992). The main difference among the proposed methods is the technique to transfer information between fine- and coarse-scale approximations.

In order to expedite 3-D problems, Duarte and Kim (2008) and Kim et al. (2008) introduced a two-scale approach using global–local enrichment functions in a GFEM framework referred to as GFEM^{g-l}. The GFEM^{g-l} has proved to be very efficient for a variety of problems with singularities (Kim et al., 2008, 2010; Pereira et al., 2010) and strongly localized gradients (O'Hara et al., 2009). The procedure involves the analysis of an initial global problem using a coarse finite element mesh in order to provide boundary conditions (BCs) to the local problems that are strategically extracted from the global domain. These local problems can use much finer meshes in order to describe features of interest (i.e. cracks, flaws, inclusions), and their solutions are used to enrich the global problem through the partition of unity framework of the GFEM. Kim et al. (2008) also applied the GFEM concepts for a Multi-Site Cracking (MSC) problem of a plate under uniaxial tension, and Kim et al. (2010) tackled an industrial problem where three cracks are solved in three-different local problems and their solutions are then passed to the global domain, one crack at a time, through enrichment functions. Kim et al. (2011) explored the natural parallelism of the GFEM global–local strategy in which

* Corresponding author. Tel.: +1 (323) 343 4455; fax: +1 (323) 343 6316.
E-mail address: fevange2@calstatela.edu (F. Evangelista Jr.).

different local problems were solved with different processors. Although the aforementioned references have demonstrated the computational accuracy and robustness of the GFEM^{g-1} approach to include more than one crack, the literature lacks extension of the method to large-scale problems involving hundreds of thousand degrees-of-freedom and multiple cracks with different orders of magnitude considered simultaneously as special enrichments in the global domain.

The main contribution of this paper is to extend the benefits of the global–local approach in the generalized finite element method framework (GFEM^{g-1}) to a broader class of three-dimensional fracture problems involving realistic boundaries conditions and existence of multiple cracks of different orders of magnitude and geometry within multiple regions of the domain. For example, the consideration of realistic shrinkage crack sizes in concrete structures lead to different scales for the problem because of the different orders of magnitude of the crack sizes relative to the entire domain. A multi-site cracking (MSC) problem is idealized for an airfield concrete slab supported by an elastic foundation and loaded by a new generation aircraft. In this large-scale problem, multiple initial cracks are assumed to be in critical positions of the slab where the existence of those cracks or flaws is likely to grow and eventually cause structural failure when combined with specific loading conditions. For example, excessive shrinkage of the concrete slab can create surface-initiated cracks of very small dimensions in conjunction with a macro-crack at the top of the slab (Heath and Roesler, 2000; Bolander and Berton, 2004; Evangelista Jr. and Roesler, 2010). The large size of airfield slabs pose difficulties to traditional numerical methods with millions of degrees-of-freedom due to the three-dimensional nature of the slab geometry, large aircraft landing gears, and crack position and size. Furthermore, traditional numerical methods generally cannot tackle this problem because as the crack size decreases, computations at the refined crack fronts become more challenging due to numerical round-off errors governed by the large domain. A large ratio of domain size and the size of the smallest finite element in a mesh leads, in general, to a large condition number of the global stiffness matrix. This ill-conditioning of the global matrix may cause severe round-off errors when using a direct solver or cause iterative solvers not to converge.

This paper proposes the formulation of a GFEM^{g-1} in a MSC framework to investigate the cracking potential of 3-D airfield concrete slabs over elastic foundation loaded by new generation aircraft. The approach considers an initial problem with a coarse mesh with a single crack, and only accounts for the presence of the other cracks in the local problem which uses a fine mesh (one local problem for each crack). The solution (displacements) of each local problem is used as enrichment functions, through the GFEM framework, in the global domain which is re-solved to account for the presence of the multiple cracks simultaneously in the enriched global domain. The key contribution is that all the special enrichment functions created from each local problem simultaneously enrich the global domain bridging the displacement effects of all the discontinuity and/or singularity of the MSC problem. Furthermore, the computational cost of the two-scale problem is significantly reduced, since only the local problem explicitly contains the features of interest and the finer mesh. The quantification of the crack growth potential of aircraft-loaded concrete slab containing multiple cracks is performed through the evaluation of crack front parameters using Linear Elastic Fracture Mechanics (LEFM) quantities, specifically Stress Intensity Factors (SIF) for the opening (K_I), in-plane (K_{II}), and out-plane shear (K_{III}) modes.

2. Generalized finite element method (GFEM)

The GFEM, or also called extended finite element method (XFEM), has shown promise in overcoming difficulties in three-dimensional crack simulations (Belytschko et al., 1996). The key technological advance of this method is that standard finite element shape functions can be locally enriched with special functions that efficiently approximate discontinuous or singular fields, i.e., cracks. The GFEM enables the insertion of crack surfaces in any position of the model without the need to fit the standard finite element mesh boundaries to the crack surface (Babuska et al., 1994; Duarte and Oden, 1996; Belytschko and Black, 1999).

The GFEM uses the concept of Partition of Unity to build new approximation functions (Babuska et al., 1994). In the GFEM framework, a shape function is built by combining a standard finite element shape function (φ_α) and an enrichment function ($L_{\alpha i}$):

$$\phi_{i\alpha}(\mathbf{x}) = \varphi_\alpha(\mathbf{x})L_{\alpha i}(\mathbf{x}) \tag{1}$$

(without a summation on α); in which α is the index for a node in the finite element mesh. Fig. 1(a) shows the construction of a 2-D GFEM shape function for a node $\mathbf{x}_\alpha$ shared by four rectangular elements as illustrated in the bottom of the figure. The function at the top is a standard linear finite element shape function φ_α, a polynomial enrichment $L_{\alpha i}$ is shown in the middle, and the resulting generalized FE shape function, $\phi_{i\alpha}$, is shown as the bottom function.

In the context of a discretized finite element domain, the GFEM approximation $\mathbf{u}^{hp}(\mathbf{x})$ of a displacement field $\mathbf{u(x)}$ is defined as:

(a) continuous high-order enrichment   (b) discontinuous high-order enrichment
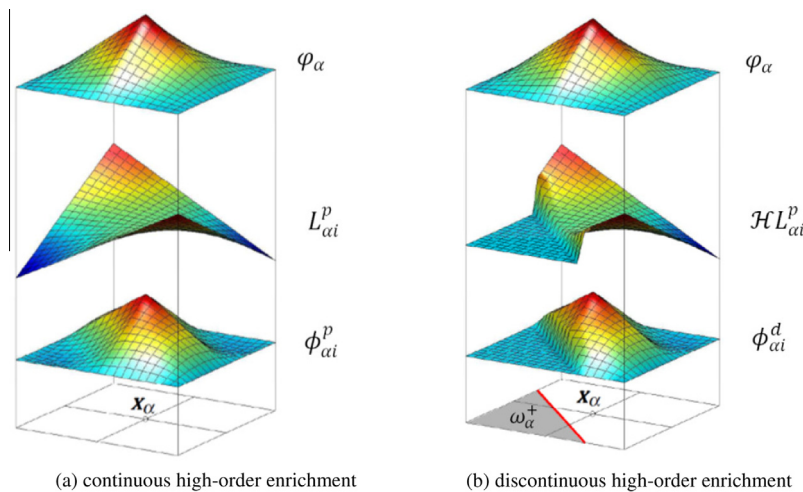
Fig. 1. GFEM shape function construction for (a) continuous and (b) discontinuous high-order enrichments.

$$\boldsymbol{u}^{hp}(\boldsymbol{x}) = \sum_{\alpha=1}^{N}\sum_{i=1}^{D_L} \boldsymbol{u}_{\alpha i}\varphi_\alpha(\boldsymbol{x})L_{\alpha i}(\boldsymbol{x}) = \sum_{\alpha=1}^{N}\varphi_\alpha(\boldsymbol{x})\sum_{i=1}^{D_L}\boldsymbol{u}_{\alpha i}L_{\alpha i}(\boldsymbol{x}) \qquad (2)$$

where $\boldsymbol{u}_{\alpha i}$ are the nodal degree-of-freedom at the element node α, N is the number of nodes, and D_L is the number of enrichment functions assigned to node α. It is important to note that $\boldsymbol{u}^{hp}(\boldsymbol{x})$ is the local approximation defined in the support domain, ω_α, which is the union of the finite element sharing the same node $\boldsymbol{x}_\alpha$, as showed in the bottom of Fig. 1(a).

In the GFEM, the enrichment functions, $L_{\alpha i}$, can be conveniently chosen to improve the local approximation with the finite element shape function. The method allows more flexibility in simulating various types of problems encountered in mechanics. For example, finite element simulations can apply polynomial enrichment functions to enable coarsening the finite element mesh without losing accuracy of the solution.

The set of polynomial enrichment functions used in this paper has a support domain, ω_α, associated with a node $\boldsymbol{x}_\alpha$ $(X_{1\alpha},X_{2\alpha},X_{3\alpha})$ and is defined in (Oden et al., 1998) as:

$$\{L_{\alpha i}^p\}_{i=1}^{\tilde{D}_L} = \left\{1, \frac{(X_1 - X_{1\alpha})}{h_\alpha}, \frac{(X_2 - X_{2\alpha})}{h_\alpha}, \frac{(X_3 - X_{3\alpha})}{h_\alpha}, \frac{(X_1 - X_{1\alpha})^2}{h_\alpha}, \frac{(X_2 - X_{2\alpha})^2}{h_\alpha}, \ldots \right\} \qquad (3)$$

where $X_{1\alpha}$, $X_{2\alpha}$, and $X_{3\alpha}$ are the coordinates for the node $\boldsymbol{x}_\alpha$; X_1, X_2, and X_3 are the coordinates of the point where the enrichment is computed; and h_α is a scaling factor. Therefore, the GFEM approximation of the continuous field $\tilde{\boldsymbol{u}}_{\alpha i}$ is:

$$\tilde{\boldsymbol{u}}_\alpha^{hp}(x) = \sum_{i=1}^{\tilde{D}_L}\tilde{\boldsymbol{u}}_{\alpha i}L_{\alpha i}^p(\boldsymbol{x}) \qquad (4)$$

In fracture mechanics applications, special functions can be used to simulate the presence of cracks without the need to tailor the finite element mesh to the crack surface and still capture the discontinuity induced by the crack surface. Therefore, discontinuous enrichment functions, $L_{\alpha i}^d$, are used for nodes at the support domain, ω_α, that intersect the crack surface but not the crack front (Duarte et al., 2007a; Pereira et al., 2010):

$$\{L_{\alpha i}^d\}_{i=1}^{\tilde{D}_L} = \mathcal{H}L_{\alpha i}^p(\boldsymbol{x}) \quad \text{with } \mathcal{H}(x) = \begin{cases} 1 & \text{if } x \in \omega_\alpha^+ \\ 0 & \text{otherwise} \end{cases} \qquad (5)$$

where ω_α^+ is the region of the support domain on one side of the discontinuity as shown by the gray area in Fig. 1(b). Thus, the GFEM approximation of the discontinuous field $\hat{u}_{\alpha i}$ can be written as:

$$\hat{u}_\alpha^{hp}(x) = \sum_{i=1}^{\tilde{D}_L}\hat{u}_{\alpha i}L_{i\alpha}^d(\boldsymbol{x}) \qquad (6)$$

Enrichment functions to model the crack front singularity can be chosen according to available solutions using LEFM, such as two-dimensional asymptotic expansions of the elastic solution for plane strain. The enrichment corresponds to the first-order terms of modes I and II, and the first and second order terms of mode III for the asymptotic expansion around a straight crack front of a traction-free flat crack surface (Szabó and Babuška, 1991; Pereira et al., 2009).

$$\left\{ \left\{\breve{L}_{\alpha j}^{\varepsilon_i}(r,\theta)\right\}_{i=1}^3 \right\}_{j=1}^2 = \begin{cases} \breve{L}_{\alpha 1}^{\varepsilon_1}(r,\theta) = \sqrt{r}\left[(\kappa - \frac{1}{2})cos\frac{\theta}{2} - \frac{1}{2}cos\frac{3\theta}{2}\right] \\ \breve{L}_{\alpha 1}^{\varepsilon_2}(r,\theta) = \sqrt{r}\left[(\kappa + \frac{1}{2})sin\frac{\theta}{2} - \frac{1}{2}sin\frac{3\theta}{2}\right] \\ \breve{L}_{\alpha 1}^{\varepsilon_3}(r,\theta) = \sqrt{r}sin\frac{\theta}{2} \\ \breve{L}_{\alpha 2}^{\varepsilon_1}(r,\theta) = \sqrt{r}\left[(\kappa + \frac{3}{2})sin\frac{\theta}{2} + \frac{1}{2}sin\frac{3\theta}{2}\right] \\ \breve{L}_{\alpha 2}^{\varepsilon_2}(r,\theta) = \sqrt{r}\left[(\kappa - \frac{3}{2})cos\frac{\theta}{2} + \frac{1}{2}cos\frac{3\theta}{2}\right] \\ \breve{L}_{\alpha 2}^{\varepsilon_3}(r,\theta) = \sqrt{r}sin\frac{3\theta}{2} \end{cases} \qquad (7)$$

where r, θ, and ε_3 are local curvilinear cylindrical coordinates; ε_1, ε_2, and ε_3 are the directions in the curvilinear coordinate system defined along the crack front; κ is a constant $\kappa = 1 - \upsilon$; and υ is the material Poisson's ratio. Therefore, the GFEM approximation of the singular field $\breve{u}_{\alpha i}^{\varepsilon_i}$ is:

$$\breve{u}_\alpha^{hp} = \sum_{i=1}^2 \begin{bmatrix} \breve{u}_{\alpha i}^{\varepsilon_1}\breve{L}_{\alpha i}^{\varepsilon_1}(r,\theta) \\ \breve{u}_{\alpha i}^{\varepsilon_2}\breve{L}_{\alpha i}^{\varepsilon_2}(r,\theta) \\ \breve{u}_{\alpha i}^{\varepsilon_3}\breve{L}_{\alpha i}^{\varepsilon_3}(r,\theta) \end{bmatrix} \qquad (8)$$

Duarte and collaborators (Duarte et al., 2007b; Pereira et al., 2009, 2010; Garzon et al., 2010) have developed a geometric and numerical engine to model and handle arbitrarily located crack surfaces in 3-D domains using the above described enrichments in a GFEM framework. Automatic refinement around the crack front is performed by detecting elements that intersect with crack surface and then enriching with singular functions for nodes immediately ahead the crack front, and discontinuous functions are used for nodes within the elements which the crack surface has passed through. Furthermore, non-uniform polynomial enrichment was also applied to the domain.

3. Two-scale strategy using the generalized finite element method

Exploring the flexibility of the GFEM in using special functions to improve the approximation, Duarte et al., 2007a; Duarte and Kim, 2008; Kim et al., 2008 introduced GFEM^{g-l} as an alternative to the standard global–local approach currently used with the finite element method. In the GFEM^{g-l}, enrichment functions are numerically built from solutions of local problems as depicted in Fig. 2. The procedure to build numerical enrichment functions, shown in the figure, can be summarized by the following steps (Duarte and Kim, 2008):

1. Solve an initial global problem.
2. Create local problem (s).
3. Provide boundary conditions to local problem (s) from the initial global problem.
4. Solve local problem (s)
5. Enrich global solution with local problem (s) solutions.
6. Solve enriched global problem.
7. Extract crack front parameters of interest such as stress intensity factors (K) or energy release rates (G).

The following sections detail the basic concepts of the GFEM^{g-l}, the construction of the global–local enrichment functions, and their relations to the GFEM strategy discussed in the previous section.

3.1. Global problem

Consider the boundary value problem (BVP) shown in Fig. 2(a). The problem consists of a global domain Ω_G with a boundary Γ_G Tractions $\bar{\boldsymbol{t}}$ and displacements $\bar{\boldsymbol{u}}$ are prescribed on the complementary surfaces Γ_G^t and Γ_G^u, respectively. The governing equations, without consideration of body forces or inertial effects, can be defined as:

$\nabla \cdot \boldsymbol{\sigma} = 0$ in Ω_G Equilibrium equations

$\boldsymbol{\sigma} \cdot n = \bar{t}$ on Γ_G^t traction boundary condition

$\boldsymbol{u} = \bar{\boldsymbol{u}}$ on Γ_G^u displacement boundary condition   (9a-e)

$\boldsymbol{\sigma} = C : \boldsymbol{\varepsilon}$ in Ω_G constitutive equations

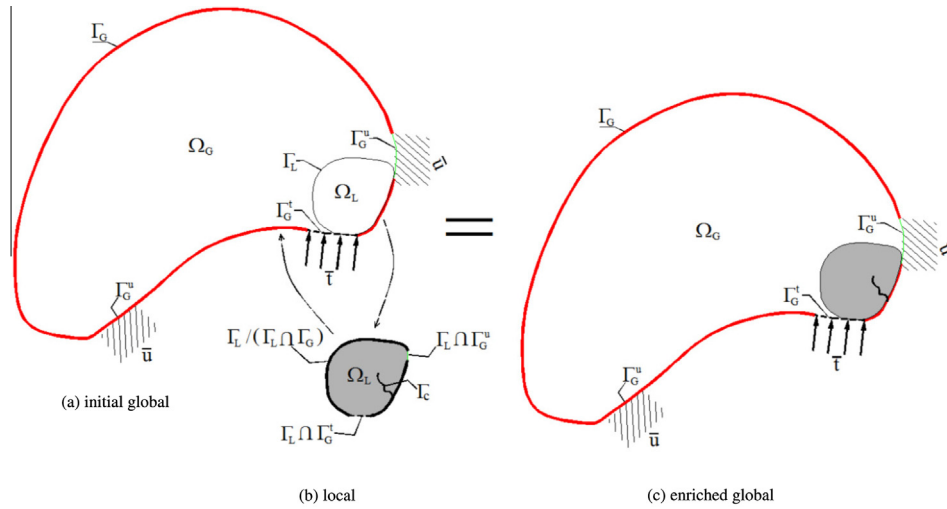$\boldsymbol{\varepsilon} = \nabla_s u$ kinematic relations

Fig. 2. GFEM^{g-1} steps for static fracture mechanics problems: (a) initial global, (b) local, and (c) enriched global problems.

where $\boldsymbol{n}$ is the outward normal vector on Γ_G^t; $\boldsymbol{\sigma}$ is the Cauchy stress tensor; $\boldsymbol{C}$ is the Hookean constitutive tensor; $\boldsymbol{\varepsilon}$ is the linear strain tensor; ∇_s is the symmetric part of the gradient operator tensor. Then, let $\boldsymbol{u}_G^0$ be the GFEM solution of the initial static problem defined in Eq. (9a-e) for the field displacement $\boldsymbol{u}$. The weak form of this problem is stated as follows:

Find $\boldsymbol{u}_G^0 \in \mathbf{X}_G^0(\Omega_G) \subset H^1(\Omega_G)$ such that $\forall \boldsymbol{v}_G^0 \in \mathbf{X}_G^0(\Omega_G)$

$$\int_{\Omega_G} \boldsymbol{\sigma}(\boldsymbol{u}_G^0) : \boldsymbol{\varepsilon}(\boldsymbol{v}_G^0) d\boldsymbol{x} + \eta \int_{\Gamma_G^u} \boldsymbol{u}_G^0 \cdot \boldsymbol{v}_G^0 ds$$
$$= \int_{\Gamma_G^t} \bar{\boldsymbol{t}} \cdot \boldsymbol{v}_G^0 ds + \eta \int_{\Gamma_G^u} \bar{\boldsymbol{u}} \cdot \boldsymbol{v}_G^0 ds \qquad (10)$$

where $\boldsymbol{v}_G^0$ are the virtual displacement, η is the penalty parameter used to assign displacement boundary conditions defined on Γ_G^u, and $\mathbf{X}_G^0(\Omega_G)$ is a discretization of the Hilbert space $H^1(\Omega_G)$ defined in Ω_G, and built using GFEM shape functions:

$$\mathbf{X}_G^0(\Omega_G) = \{\tilde{\boldsymbol{u}}_\alpha^{hp}\} \qquad (11)$$

where $\tilde{\boldsymbol{u}}_{\alpha i}^{hp}$ is defined in Eq. (4). The search for the unknown degrees-of-freedom of $\boldsymbol{u}_G^0$ is led through Eq. (10) to a system of linear equations.

3.2. Local problem

Let $\boldsymbol{u}_L$ be the GFEM solution of the local problem containing a crack surface Γ_c as shown in Fig. 2(b). The problem is solved on a subdomain Ω_L of the global domain Ω_G after the global solution $\boldsymbol{u}_G^0$ is computed as described in the previous section. The weak form of the local problem can be stated as follows

Find $\boldsymbol{u}_L \in \mathbf{X}_L^{hp}(\Omega_L) \subset H^1(\Omega_L)$ such that $\forall \boldsymbol{v}_L \in \mathbf{X}_L^{hp}(\Omega_L)$

$$\int_{\Omega_L} \boldsymbol{\sigma}(\boldsymbol{u}_L) : \boldsymbol{\varepsilon}(\boldsymbol{v}_L) d\boldsymbol{x} + \eta \int_{\Gamma_L \cap \Gamma_G^u} \boldsymbol{u}_L \cdot \boldsymbol{v}_L ds + \kappa \int_{\Gamma_L/(\Gamma_L \cap \Gamma_G)} \boldsymbol{u}_L \cdot \boldsymbol{v}_L ds$$
$$= \int_{\Gamma_L \cap \Gamma_G^t} \bar{\boldsymbol{t}} \cdot \boldsymbol{v}_L ds + \eta \int_{\Gamma_L \cap \Gamma_G^u} \bar{\boldsymbol{u}} \cdot \boldsymbol{v}_L ds + \int_{\Gamma_L/(\Gamma_L \cap \Gamma_G)} (n \cdot \boldsymbol{\sigma}(\boldsymbol{u}_G^0)$$
$$+ \kappa \boldsymbol{u}_G^0) \cdot \boldsymbol{v}_L ds \qquad (12)$$

where η is the penalty parameter used to assign displacement boundary conditions defined on $\Gamma_L \cap \Gamma_G^u$, κ is the spring stiffness used to assign boundary conditions defined on $\Gamma_L/(\Gamma_L \cap \Gamma_G)$, and $\mathbf{X}_L^{hp}(\Omega_L)$ is a discretization of the Hilbert space $H^1(\Omega_L)$ defined in Ω_L.

In fracture mechanics problems with the presence of a crack in the local domain, the space $\mathbf{X}_L^{hp}(\Omega_L)$ has GFEM shape functions built

with discontinuous and singular enrichments, and Eq. (12) is solved in the same way as in the global problem. The type of boundaries conditions provided by $\boldsymbol{u}_G^0$ depends on the choice of the parameters η and κ. For example, Neumann boundary conditions (tractions) are prescribed on $\Gamma_L/(\Gamma_L \cap \Gamma_G)$ if $\kappa = 0$. Dirichlet boundary conditions (the displacement solution $\boldsymbol{u} - G^0$) are prescribed on $\Gamma_L/(\Gamma_L \cap \Gamma_G)$ if $\kappa = \eta \gg 1$. Since the solution of the initial global problem $\boldsymbol{u}_G^0$ can be considered accurate enough and smooth away from the crack fronts, it can be used as boundary condition on $\Gamma_L/(\Gamma_L \cap \Gamma_G)$ of the global problem (Duarte and Kim 2008). On the portions of Ω_L that intersect the global problem (Ω_G^u or Ω_G^t), exact boundary conditions are applied. It is important to note that, in the GFEM^{g-1} approach described here, quantities of interest such as SIFs are not evaluated in the local domain but evaluated back in the global domain enriched with the local solution $\boldsymbol{u}_L$ solved from Eq. (12).

3.3. Enriched global problem

The local solution $\boldsymbol{u}_L$ is used as enrichment function in the global coarse mesh through global–local generalized finite element shape functions:

$$\phi_\alpha(\boldsymbol{x}) = \varphi_\alpha(\boldsymbol{x})\boldsymbol{u}_L(\boldsymbol{x}) \qquad (13)$$

where $\varphi_\alpha(\boldsymbol{x})$ is the finite element shape function used at node $\boldsymbol{x}_\alpha$, whose support ω_α is contained in the domain Ω_L. Then, the global problem (defined in Section 3.1) can be solved again using Eq. (13) finally leading to the solution $\boldsymbol{u}_G^E$. This enriched global solution is illustrated in Fig. 2(c). Duarte and Kim (2008) further proposed a technique to efficiently solve the linear system for $\boldsymbol{u}_G^E$ using the available factorization of the global stiffness matrix of the initial global problem. It is shown that the CPU time required to solve the enriched global problem is approximately 5% of the time required to solve the initial global one. More details about this technique can be found in Duarte and Kim (2008) and Kim et al. (2010).

The accuracy of the GFEM^{g-1} is not significantly affected by the size of the local domains as shown in Duarte and Kim (2008). The authors suggest the use of local domains in which the crack front is not close to the local boundary. If the global mesh is coarse, which is in general the case, this requirement on the local domain is automatically satisfied. Alternatively, the iterative procedure proposed in Gupta et al. (2012) can be used to control the accuracy of the GFEM^{g-1} regardless of the local domain size.

4. Three-dimensional MSC modeling for airfield slabs

4.1. Finite element model

A large scale three-dimensional problem is shown in Fig. 3(a) and (b) where an A-380 aircraft and its two triple dual tandem (TDT) gears loads an airfield concrete slab. An idealized MSC problem and finite element mesh, is shown in Fig. 3(c), at a potential critical loading position with one of the TDT belly gears placed in one corner of the slab, while half of the other TDT gear loads the other corner. The critical positions for the airfield slab are selected according to previous 2D and 3D analyses of Evangelista Jr. and Roesler (2009) and Evangelista Jr. and Roesler (2010). A major through-the-length crack is assumed at the

position of maximum tensile stress on the top of the slab. Several other cracks are placed in critical locations for different stress conditions such as compression, tensile, shear, and combined stress situations. The surface cracks are idealized as existing cracks and can be attributed to combined material-environmental effects such as concrete shrinkage cracks which are more likely to occur at early ages than bottom-initiated fatigue cracks (Heath and Roesler, 2000; Bolander and Berton, 2004; Rao and Roesler, 2005). The small crack surface placed at the bottom of the slab is rotated 45° relative to the bottom of the slab in order to investigate possible mixed-modality due to the high compression at the bottom of the slab at that location. Fig. 3(d) shows the cross-section with the boundary conditions and material properties.

(a) aircraft A-380 (source: www.airliners.net)

(b) detail of the belly gears with the two TDT gears
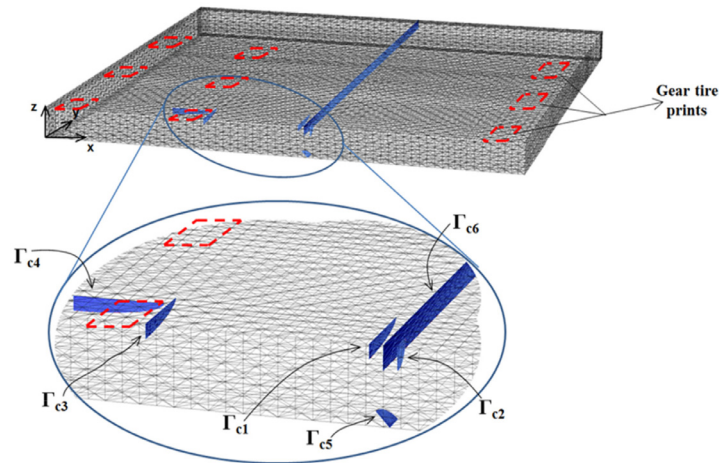
(c) MSC idealization with aircraft loading and assumed existing surface cracks
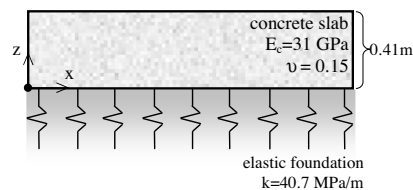
(d) cross-section, boundary conditions, and material properties

Fig. 3. Airfield problem with (a) new generation aircraft A-380; (b) detail of the belly gears with two triple dual tandems (TDT); (c) slab mesh, load position for the TDT belly gears, and position of potential cracks defining the MSC problem; (d) cross-section of the slab with boundary conditions and material properties.

(a) rectangular crack for top of the slab (Γ_{c6})

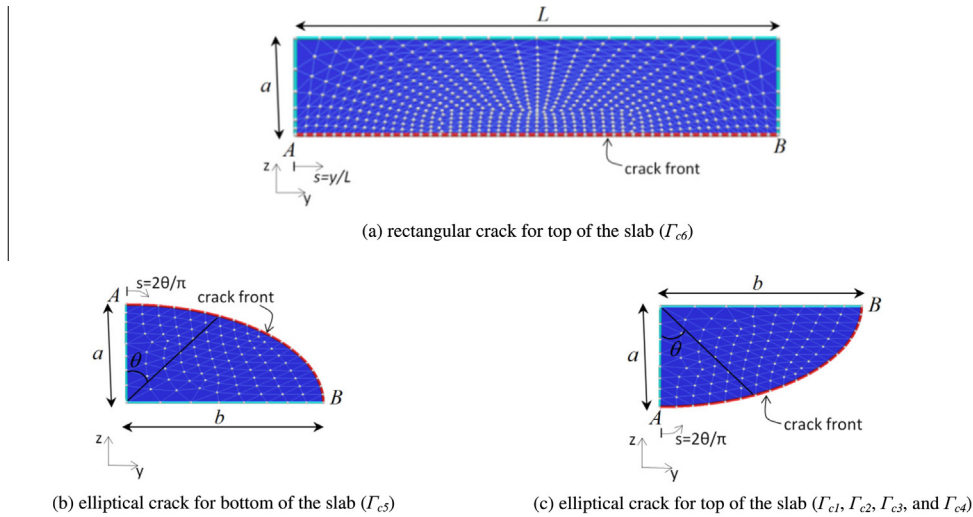(b) elliptical crack for bottom of the slab (Γ_{c5})

(c) elliptical crack for top of the slab (Γ_{c1}, Γ_{c2}, Γ_{c3}, and Γ_{c4})

Fig. 4. Geometry for rectangular and quarter-elliptical surfaces for (a) and (c) surface-initiated cracks; and (b) bottom-initiated crack.

Table 1
Crack surface geometry.

Crack	Γ_{c1}	Γ_{c2}	Γ_{c3}	Γ_{c4}	Γ_{c5}	Γ_{c6}
Type	Quarter-elliptical	Quarter-elliptical	Quarter-elliptical	Quarter-elliptical	Quarter-elliptical	Rectangular
$a \times b$ (mm^2)	76×508	127×152	76×508	76×508	76×127	127×6100
$a_e{}^a$ (mm)	113	80	113	113	57	880

^{a} $a_e = \sqrt{A}$, with A the area of the crack surface.

Fig. 4 presents the geometry of the idealized crack surfaces shown in Fig. 3(c). The cracks are rectangular and quarter-elliptical surfaces with depth a and length b, and the normalized variable, s, varying from 0 to 1, which defines the local position along the crack front ($\bar{AB}$). Table 1 lists the specific details of the geometry type and dimensions (a and b) of the six cracks (Γ_{c1} to Γ_{c6}) for the slab configuration loaded with the TDT aircraft gears. An equivalent crack length a_e is also determined to express a characteristic size for each crack surface. The values of a_e spans in two different orders of magnitude due to the different sizes of cracks considered for the MSC problem.

As shown in Fig. 4, 2D triangular elements are only used to represent the crack surface geometry to be inserted in the 3D model of the slab. The nodes do not have degrees of freedom like standard finite elements and the crack surface mesh is independent of the 3D finite element mesh (Duarte et al., 2000). For the surface-initiated cracks (Fig. 4(a) and (c)), the crack front is at the bottom of the crack surfaces, which promotes top-down cracking in the slab for the critical gear load location. Similarly, for the bottom-initiated crack (Fig. 4(b)), the crack front is at the top of the crack surface inducing bottom-up cracking.

4.2. Two-scale approach

The multi-site cracking problem described previously is solved with GFEM^{g-1} strategy based on the general formulation in Section 3. The flowchart in Fig. 5 summarizes the domains, surfaces, and enrichments used for the initial global, local, and the enriched global problems. The initial global problem only has the rectangular through-the-length crack, Γ_{c6} explicitly modeled. All the other crack surfaces, Γ_{c1} to Γ_{c5}, are simulated in independent local problems, and their effects are passed to the global problem through the global–local enrichment functions ($\{u_L^i\}_{i=1}^5$) when solving the enriched global problem. These enrichments are applied to the nodes of the global mesh that comprise the local problems according to Eq. (13). Therefore, the resulting enriched global problem

has just one crack explicitly modeled but has also the kinematics of the five other cracks modeled simultaneously.

The initial global problem is solved with a coarse mesh of four-node tetrahedral volume elements for the domain discretization. Fig. 6 shows the slab's finite element mesh and stress distribution (σ_{xx}) for the initial global problem loaded with the aircraft belly gears from Fig. 3(c). As seen in Fig. 6, the global slab model only has the single crack (through-the-length) explicitly modeled. Fig. 6 also shows each local problem created to analyze the effects of the individual crack surfaces with respect to the global loading conditions, and their respective meshes and stress solution. The coarse mesh shown for each local problem is the respective global mesh at that position while the finer mesh is used to solve the local problem with the respective crack explicitly modeled. The opening at each crack site can also be observed since the displacements are magnified 500 times.

Although GFEM enrichment functions provide better solutions for coarser meshes relative to the standard FEM, local problem, mesh refinement is still required at elements close to the crack front. Therefore coarse mesh for each local problem is inherited from the initial global problem while the fine mesh is obtained through additional local refinement, as seen in Fig. 6. Specifically, mesh refinement was completed for elements that intersect the crack surface or crack vertices in order to have the ratio of the longest edge of the element (ℓ_e) to the equivalent crack size (a_e) along the crack front approximately $0.1 \geqslant \ell_e/a_e \geqslant 0.02$.

Table 2 lists the mesh size parameters for the crack front of each crack considered for the MSC problem. The quantity ℓ_e/L_{slab} expresses the ratio of ℓ_e to the size of the entire domain represented here as the slab size (L_{slab}). The ratios span three orders of magnitude ($10^{-5} \leqslant \ell_e/L_{slab} \leqslant 10^{-2}$) showing that as the crack size decreases, the computations increase due to the more refined crack fronts. Traditional numerical methods such as the standard finite element method, generally cannot handle this specific problem due to numerical round-off errors.
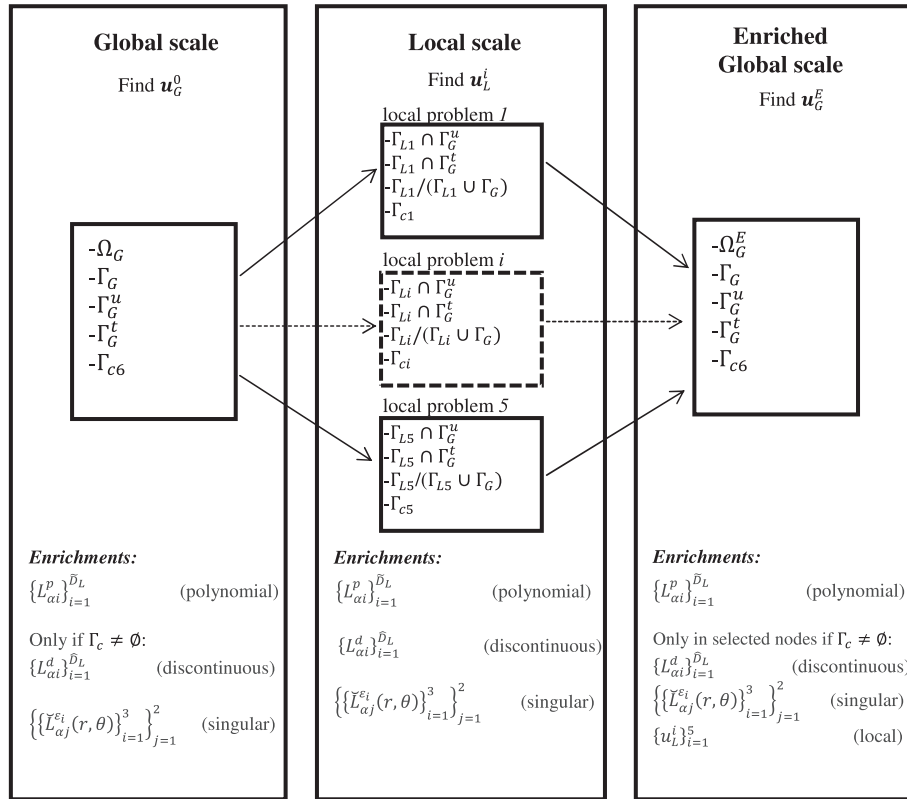
Global scale

Find $\boldsymbol{u}_G^0$

- Ω_G
- Γ_G
- Γ_G^u
- Γ_G^t
- Γ_{c6}

Enrichments:

$\{L_{\alpha i}^p\}_{i=1}^{\tilde{D}_L}$　　　(polynomial)

Only if $\Gamma_c \neq \emptyset$:

$\{L_{\alpha i}^d\}_{i=1}^{\tilde{D}_L}$　　　(discontinuous)

$\left\{\{\tilde{L}_{\alpha j}^{\varepsilon_i}(r,\theta)\}_{i=1}^3\right\}_{j=1}^2$　　(singular)

Local scale

Find $\boldsymbol{u}_L^i$

local problem *1*
- $\Gamma_{L1} \cap \Gamma_G^u$
- $\Gamma_{L1} \cap \Gamma_G^t$
- $\Gamma_{L1}/(\Gamma_{L1} \cup \Gamma_G)$
- Γ_{c1}

local problem *i*
- $\Gamma_{Li} \cap \Gamma_G^u$
- $\Gamma_{Li} \cap \Gamma_G^t$
- $\Gamma_{Li}/(\Gamma_{Li} \cup \Gamma_G)$
- Γ_{ci}

local problem *5*
- $\Gamma_{L5} \cap \Gamma_G^u$
- $\Gamma_{L5} \cap \Gamma_G^t$
- $\Gamma_{L5}/(\Gamma_{L5} \cup \Gamma_G)$
- Γ_{c5}

Enrichments:

$\{L_{\alpha i}^p\}_{i=1}^{\tilde{D}_L}$　　　(polynomial)

$\{L_{\alpha i}^d\}_{i=1}^{\tilde{D}_L}$　　　(discontinuous)

$\left\{\{\tilde{L}_{\alpha j}^{\varepsilon_i}(r,\theta)\}_{i=1}^3\right\}_{j=1}^2$　　(singular)

Enriched Global scale

Find $\boldsymbol{u}_G^E$

- Ω_G^E
- Γ_G
- Γ_G^u
- Γ_G^t
- Γ_{c6}

Enrichments:

$\{L_{\alpha i}^p\}_{i=1}^{\tilde{D}_L}$　　　(polynomial)

Only in selected nodes if $\Gamma_c \neq \emptyset$:

$\{L_{\alpha i}^d\}_{i=1}^{\tilde{D}_L}$　　　(discontinuous)

$\left\{\{\tilde{L}_{\alpha j}^{\varepsilon_i}(r,\theta)\}_{i=1}^3\right\}_{j=1}^2$　　(singular)

$\{u_L^i\}_{i=1}^5$　　　(local)

Fig. 5. Flowchart of the proposed two-scale GFEM^{g-l} strategy for the MSC problem.

Local problem Ω_{L4}

coarse mesh

fine mesh

solution

Local problem Ω_{L1}

coarse mesh　　fine mesh　　solution

Global crack Γ_{c6}

Local problem Ω_{L2}

coarse mesh　　fine mesh　　solution

Local problem Ω_{L3}

coarse mesh　　fine mesh　　solution

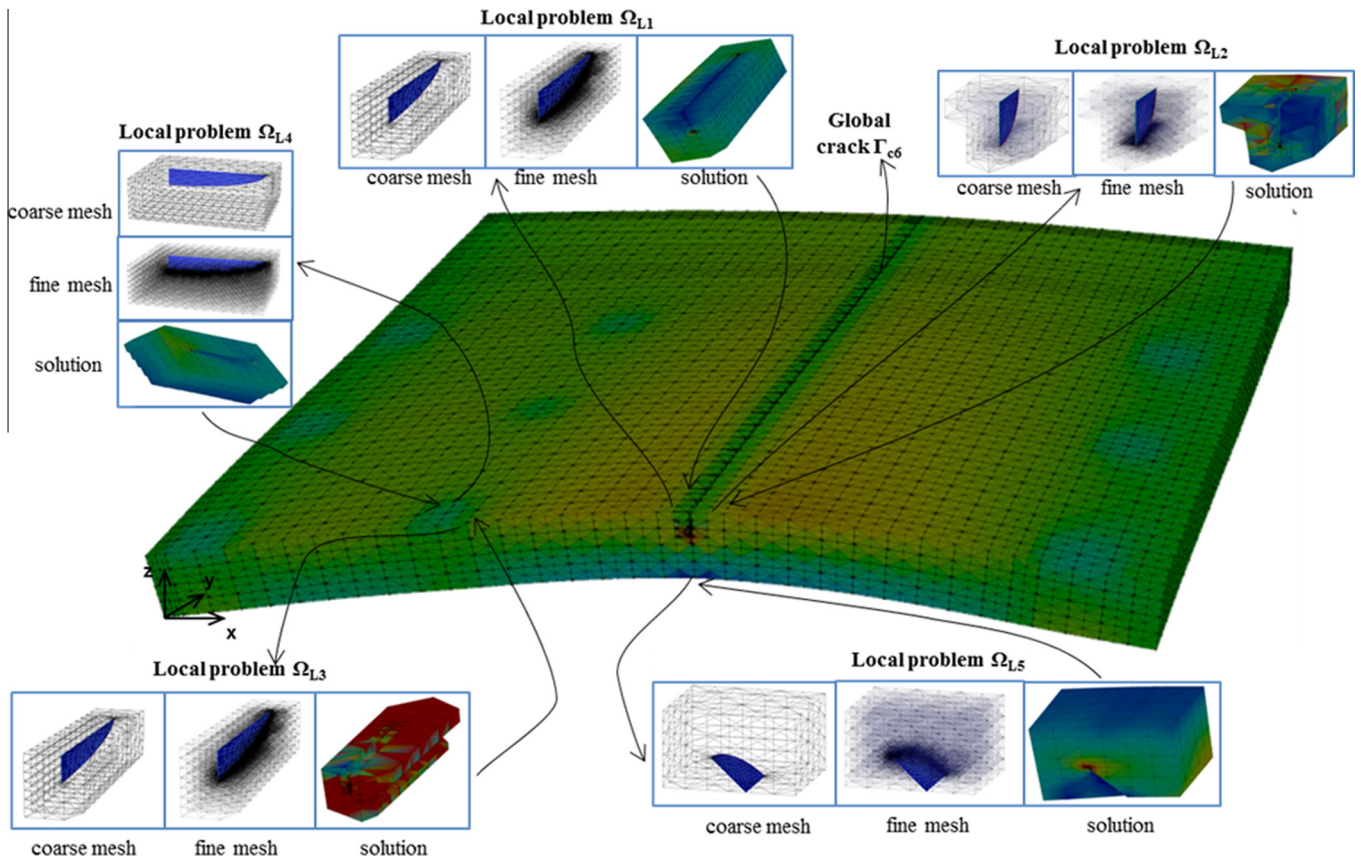Local problem Ω_{L5}

coarse mesh　　fine mesh　　solution

Fig. 6. Deformed mesh and stress distribution (σ_{xx}) for the initial global problem and position of local problems with their respective coarse and fine meshes, deformed mesh and stress solution for each crack of the MSC problem. Displacements are magnified *500* times.

Table 2
Mesh size parameters for the crack front.

Crack	Γ_{c1}	Γ_{c2}	Γ_{c3}	Γ_{c4}	Γ_{c5}	Γ_{c6}
ℓ_e (mm)	3.23	1.60	3.29	3.29	0.57	26.40
ℓ_e/L_{slab}	5.3E−04	2.6E−04	5.4E−04	5.4E−04	9.3E−05	4.3E−03

Table 3
Size of each problem through the number of degrees-of-freedom.

Problem	Mesh I	Mesh II	Reference mesh
Initial global	53,301	222,607	724,698
Local 1 (Γ_{c1})	90,689	92,689	139,603[a]
Local 2 (Γ_{c2})	57,693	59,793	98,127[a]
Global–local enrichment	8,579	9,317	20,228
Enriched global	61,880	231,924	744,926
Total	263,563	607,013	1,707,354

[a] Finer mesh refinement compared to mesh II is applied to each local problem.

5. Analysis of crack front parameters for MSC locations

The displacements of all six crack surfaces (Γ_{c1} to Γ_{c6}) are present in the domain of the enriched global problem. Therefore, the crack front parameters, such as SIFs for the three modes, are extracted using the cut-off function method (CFM) fully presented in references Szabó and Babuška (1991) and Pereira and Duarte (2006). In the CFM, a smooth extraction function is used along with the displacements of the finite element solution to calculate the stress intensity factors through evaluations of contour integrals ahead of the crack front (Szabó and Babuška, 1991). The following section presents validation and mesh convergence studies for the MSC approach followed by the results for each crack position in the global model.

5.1. Verification and mesh convergence

The convergence and accuracy of the GFEM^{g-1} solution for the crack simulations are evaluated in terms of mode I SIFs extracted for the surface-initiated quarter-elliptical cracks, Γ_{c1} and Γ_{c2}, with the TDT belly gear loading as shown in Fig. 6. Two different levels of mesh discretization for both local and global problems are compared with a reference solution with a highly refined mesh. The computational efficiency of the proposed two-scale MSC approach is then compared with traditional finite element approaches.

(i) *Mesh I*: coarse mesh of linear 4-noded tetrahedrons and enriched to a polynomial order $p = 1$ for the initial global; fine mesh and $p = 3$ for the local problems; coarse mesh and polynomial order $p = 1$ for the enriched global plus the global–local enrichments for the nodes which comprise the local problems.
(ii) *Mesh II*: coarse mesh of linear 4-noded tetrahedrons and enriched to a polynomial order $p = 2$ for the initial global; finer mesh and $p = 3$ for the local problems; coarse mesh and polynomial order $p = 2$ for the enriched global plus the global–local enrichments for the nodes which comprise the local problems.
(iii) *Reference mesh*: Coarse mesh of linear 4-noded tetrahedrons and enriched to a polynomial order $p = 3$ for the initial global; fine mesh and $p = 3$ for the local problems; coarse mesh and polynomial order $p = 3$ for the enriched global plus the global–local enrichments for the nodes which comprise the local problems

The size of the initial global problem, local problem and enriched global problem in terms of degrees-of-freedom are shown in Table 3. The quality of the initial global problem has been shown to be essential to the accuracy of the global–local approach. Therefore, the amount of refinement and polynomial order for the local problems are kept virtually the same for both meshes following recommendation of Kim et al. (2010). However different polynomial orders are used for the initial global problem in order to observe the influence of the quality of the initial global problem approximation. Even though the solution of the local problems enriches all the nodes of the global mesh that constitute each local domain, relatively few degrees-of-freedom are added to the enriched global problem.

For all the mesh configurations, the SIFs are extracted at each crack front vertex (j) for a total number of vertices (N_{ver}), as illustrated in Fig. 4(c). Fig. 7 shows the extracted mode I SIFs (y-axis) for the three meshes and two top-initiated quarter-elliptical cracks (Γ_{c1} and Γ_{c2}) for the slab loaded by the aircraft. The x-axis in Fig. 7 is the normalized variable s, which describes the position along the crack front as depicted in Fig. 4(c). The increasing mesh quality of the initial global problems, through higher polynomial order, led to the convergence of the K_I along the crack front relative to the reference mesh. Mesh II provided a very good K_I approximation with lower polynomial order and DOFs when compared to the reference mesh.

In order to quantify the relative difference of the SIFs extracted along each crack front, the error, e, is computed as the normalized discrete L^2-norm of the relative difference between the extracted SIF for the meshes I or II (K_I^j) and the reference mesh ($\tilde{K}_I^j$).

$$e = \frac{||e_i||_{L^2}}{||K_i||_{L^2}} = \frac{\sqrt{\sum_{j=1}^{N^{ver}} (K_I^j - \tilde{K}_I^j)^2}}{\sqrt{\sum_{j=1}^{N^{ver}} (\tilde{K}_I^j)^2}} \tag{14}$$

The normalized errors for both cracks are presented in Table 4 for each mesh type. The results show that mesh II provide a very small normalized error and can be regarded as adequate to be used in the modeling. The increase of the polynomial order for the initial global problem significantly decreased the normalized error for mesh II solution about 9 to 11 times compared to mesh I which verifies the conclusions of Kim et al. (2010).

5.2. Crack front parameters results

Based on the mesh verification study, mesh II is used to study the effect of crack front geometries on the SIFs for the MSC problem. Fig. 8 shows the three SIFs (left y-axis) for the slab loaded by the TDT belly gears for the six crack surfaces (a through f) comprising the MSC problem. The ratio between the mode I SIF (K_I) and an equivalent SIF (K_{eff}) calculated from the K_I, K_{II}, and K_{III} is also plotted to provide an idea of the mix-modality along the crack front. The magnitude of the ratios $|K_I/K_{eff}|$ is shown on the second y-axis to the right. The determination of K_{eff} follows Tanaka (1974) who obtains the effective SIF based on the critical value of the displacement behind the crack tip:

$$K_{eff} = \left[K_I^4 + 8K_{II}^4 + \frac{8K_{III}^4}{1-\upsilon} \right]^{1/4} \tag{15}$$

where υ is the Poisson's ratio. This definition for K_{eff} is chosen because for pure Mode II conditions, it leads to $K_{eff} = 1.68K_{II}$ which approaches the ratio $\frac{K_{eff}}{K_{II}} = 1.60$ that maximizes the energy release rate G at the propagation angle of $\theta = \pm75°$ for pure mode II fracture (Hussain et al. 1974).

The x-axis in Fig. 8 is the normalized crack front position variable, s, and the y-axis scale is chosen in order to compare the magnitude of SIF and $|K_I/K_{eff}|$ ratio among the different crack geometries and locations. A moving-least-square (MLS) technique
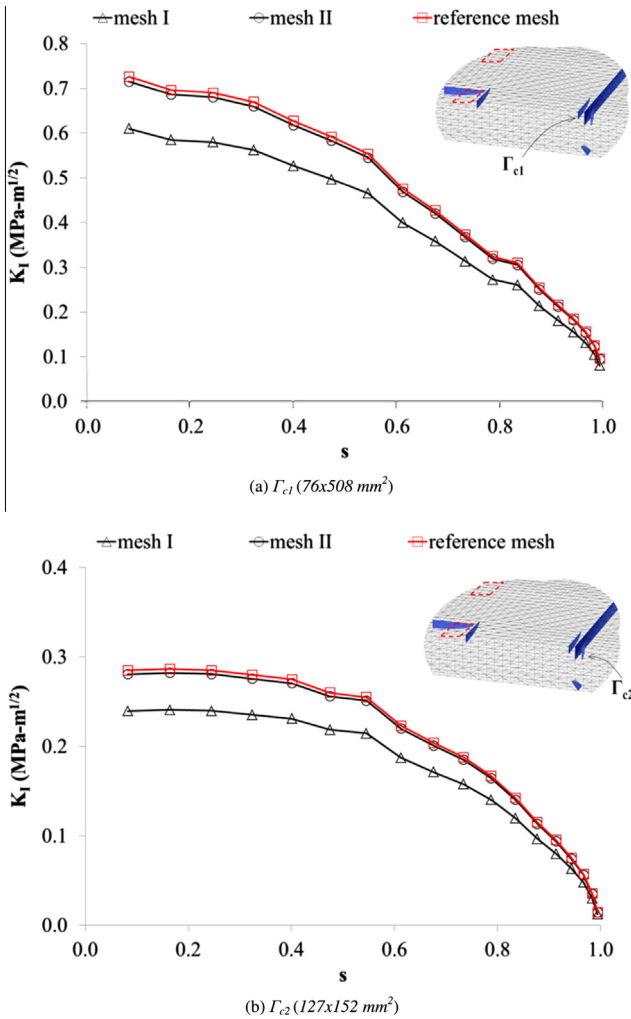
(a) Γ_{c1} (76x508 mm^2)

(b) Γ_{c2} (127x152 mm^2)

Fig. 7. Stress Intensity factors versus normalized position along the quarter-elliptical crack front (s) for top-initiated cracks (a) Γ_{c1} (76 × 508 mm^2) and (b) Γ_{c2} (127 × 152 mm^2) with TDT single gear load.

Table 4
Mesh refinement normalized error, e, for extracted SIF.

Cracks	Mesh I	Mesh II
Γ_{c1}	0.163	0.019
Γ_{c2}	0.160	0.014

is used to have a continuous and smooth representation of the SIFs along the crack front (Lancaster and Salkauskas, 1981, 1986). The MLS approximation also eliminates some noise in the results, especially for non-dominant fracture modes (Pereira, 2010).

Three idealized surface-initiated cracks (Γ_{c1}, Γ_{c2}, and Γ_{c6}) placed between the two TDT gears at the edge (Fig. 8(a),(b) and (f)) mimics concrete shrinkage cracking which is more likely to occur at early-ages than bottom-initiated fatigue cracks. The maximum K_I occurs at the edge of the slab ($s = 0$) for all three cracks, and decreases along the crack front as $s \to 1$. The magnitude of K_I also increases with the size of the initial crack length with a maximum $K_I = 2.3$ MPa m$^{1/2}$ for the through-the-length crack, Γ_{c6}.

The magnitude of the shear modes, K_{II} and K_{III}, for cracks Γ_{c1} and Γ_{c2} indicates the mixed modality of these surface cracks. Although the shear mode magnitudes are still smaller than their

respective K_I values, the magnitude of the in-plane shear increases for the crack front away from the slab edge and approaching the top-surface of the slab ($s \to 1$). Crack Γ_{c2} produces the highest K_{II} (0.3 MPa m$^{1/2}$) for $s = 1$ which also increases the mixed-modality confirmed by the $|K_I/K_{eff}|$ plot, where the ratio averages 0.8 for the crack front but dramatically decreases when $s > 0.85$. The rectangular through-the-length crack (Γ_{c6}) presents a constant $|K_I/K_{eff}| = 1$ demonstrating that this crack is approximately in mode I over the entire crack front.

Fig. 8(c) and (d) show the extracted SIFs for the surface cracks placed beside one of the TDT wheels (Γ_{c3} and Γ_{c4}), where the shear stresses are maximum. For these two crack locations and load configuration, a mixed-modality can be observed with the presence of the three modes of fracture along the crack fronts. The mode I distribution for the crack Γ_{c3} shows the crack opening conditions for this loading configuration. The $|K_I/K_{eff}|$ plots in Fig. 8(c) and (d) confirm this high mix-modality for the crack Γ_{c2}, especially when the crack front approaches the top-surface of the slab ($s \to 1$).

Finally, Fig. 8(e) shows the small crack surface (Γ_{c5}) placed at the location of maximum compression at the bottom of the slab and rotated 45° left of the normal axis of the bottom of the slab (see Fig. 6). The high compressive stress state induces negative mode I with the mixed modality observed for the entire crack front as confirmed by the $|K_I/K_{eff}|$ ratio. The maximum mixed-mode is observed at the bottom surface of the slab ($s \to 1$). The negative K_I values indicate that some interpenetration occurred at the finite element mesh nodes, which qualitatively means crack closure exists.

5.3. Computational efficiency of two-scale MSC approach

The computational efficiency of the GFEM^{g-l} to solve the MSC type of problems presented in Section 5.2 are compared, in terms of the total number of degrees-of-freedom, with two other traditional approaches.

(i) *GFEM^{g-l}*: coarse mesh of 4-noded tetrahedrons enriched to a polynomial order $p = 2$ for the initial global problem; fine mesh and $p = 3$ for the local problems; coarse mesh and polynomial order $p = 2$ for the enriched global problem plus the global–local enrichments for the nodes which comprise the local problems. Although just one crack is explicitly modeled in the global domain, all the other five cracks are considered through enrichment functions from their respective local problems.

(ii) *FEM I*: coarse mesh of 4-noded tetrahedrons and polynomial order $p = 3$ for the entire domain and localized refinement around the crack locations. All six cracks are explicitly modeled in the domain. Although p-hierarchical enrichment is applied to all nodes in the domain, this mesh aims to represent standard cubic 20-noded tetrahedrons used in the standard FEM.

(iii) *FEM II*: coarse mesh of 4-noded tetrahedrons and polynomial order $p = 2$ for the entire domain and localized refinement around the crack locations. Each crack is considered in the global domain separately, and the global problem is solved independently for each crack configuration.

The meshes for each model were constructed for both FEM I and II since the total number of degrees-of-freedom gives a good measure of the computational cost to solve each problem. Fig. 9 shows the total number of degrees-of-freedom for each method to discretize the MSC problem for the slab loaded by the TDT belly gears (Fig. 3(b)). The plot shows that the two-scale approach of the GFEM^{g-l} uses the fewest number of degrees-of-freedom among the three solution techniques. This is a result of being able to apply only a higher-order approximation to the local crack problem and
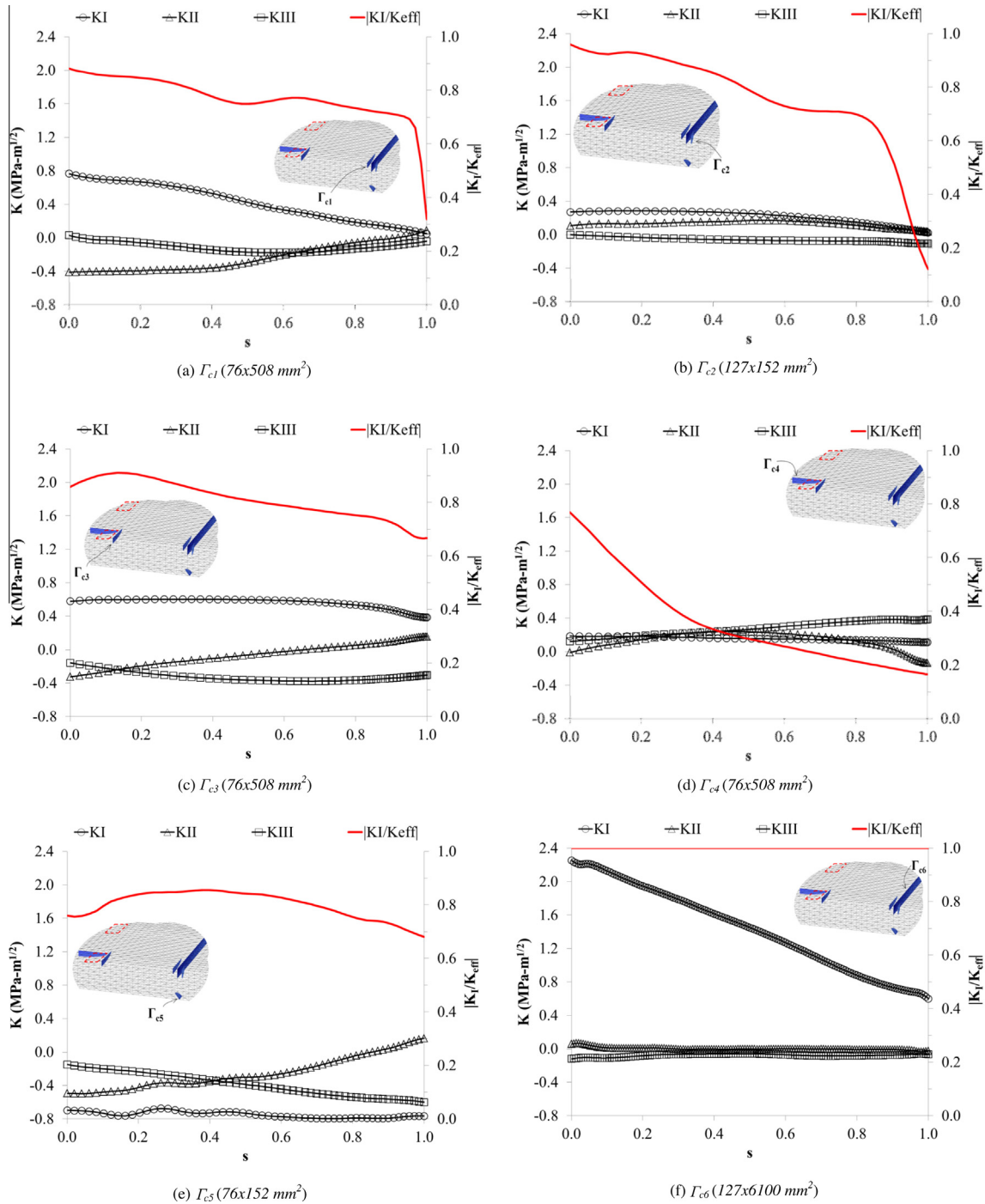
Fig. 8. Stress Intensity factors (K) and ratios $|K_I/K_{eff}|$ for surface- and bottom-initiated cracks for the slab loaded by the TDT belly gears.

not to the entire global domain. Only a small number of degrees-of-freedom are added to the enriched global problem in the two-scale approach in order to account for the simultaneous presence of all six cracks. The enriched problem is therefore just slightly larger than the initial global one. In the FEM I strategy, cubic polynomial orders for the entire global domain lead to a significant increase in the problem size. This result agrees with the efficiency of the GFEM^{g-1} reported in literature (Duarte and KIM 2008; Kim et al., 2010). (Kim et al. (2010) further emphasizes the efficiency of the GFEM^{g-1} in terms of CPU time required to solve the enriched global problem since the cost to compute the enriched global solutions cor-

responds to only 4° to 6° of the time required to solve the initial global problem. This is mainly due to the fact that the factorized stiffness matrix of the initial global problem can be used to compute the solution of the enriched global problems by static condensation, which leads to significantly lower computational cost compared with standard FEM and conventional global–local methods. Fig. 9 also shows that the FEM II strategy leads to a high computational costs when a large number of crack configurations must be analyzed independently. Furthermore, this strategy does not have the ability to capture any interaction between cracks fronts close to each other since it simulates each crack separately.
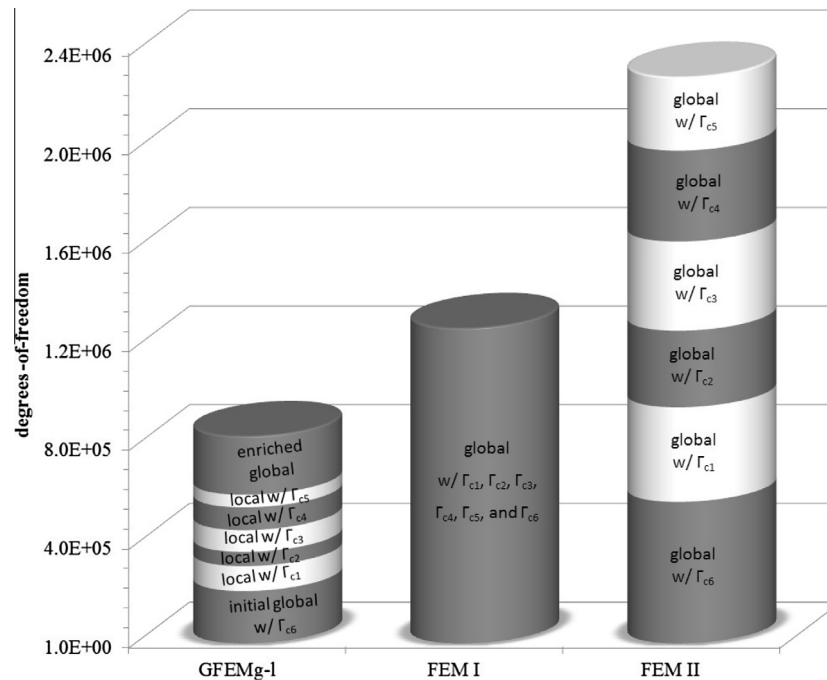
Fig. 9. Number of degrees-of-freedom used to discretize the MSC problem with six cracks within the airfield concrete slab according to three solution approaches: (i) GFEM^{g-l}, (ii) FEM I, and (iii) FEM II.

6. Conclusions

The potential for crack propagation in a realistic, large scale 3-D problem was analyzed using the generalized finite element method (GFEM) in a two-scale, multi-site cracking (MSC) approach. The global–local approach (GFEM^{g-l}) was extended to a large-scale problem where different crack geometries spanning two orders of magnitude in size were placed at different positions in a slab and loaded with the landing gears of a wide-body aircraft. Both bottom and surface-initiated cracks of varying length and geometries were inserted into multiple locations in the airport concrete slab to demonstrate the robustness of this approach. For the triple dual tandem load position analyzed, the GFEM^{g-l} showed that the surface-initiated cracks, placed at the mid-slab edge, produced the greatest crack front stress intensity factors (SIF) in the slabs. The rectangular through-the-length crack induced the highest K values with mode I dominating. Although high mixed modality existed for the cracks placed in the position of maximum shear and compressive stress states, the magnitude of the crack front SIFs were not be sufficient to propagate a mixed-mode crack. The GFEM^{g-l} allowed the displacements of multiple cracks to be represented in the global domain through enrichment functions from the local problems rather than explicitly model each crack in the global domain. The proposed strategy proved it was possible to solve an engineering-scale problem with realistic boundary conditions and initial crack conditions that traditional numerical methods generally cannot tackle due to numerical round-off errors. In addition, the two-scale approach significantly reduced the computational costs for this three-dimensional MSC problem which would have required solving over a million degrees-of-freedom problem.

Acknowledgments

References

Babuska, I., Caloz, G., Osborn, J.E., 1994. Special finite element methods for a class of second order elliptic problems with rough coefficients. SIAM Journal on Numerical Analysis 31 (4), 945–981.

Belytschko, T.B., Black, T., 1999. Elastic crack growth in finite elements with minimal remeshing. International Journal for Numerical Methods in Engineering 45 (5), 601–620.

Belytschko, T., Krongauz, Y., Organ, D., Fleming, M., Krysl, M., 1996. Meshless methods: an overview and recent developments. Computer Methods in Applied Mechanics and Engineering 139, 3–47.

Bolander, J.E., Berton, S., 2004. Simulation of shrinkage induced cracking in cement composite overlays. Cement & Concrete Composites 26, 861–871.

Diamantoudis, A.T., Labeas, G.N., 2005 (Stress intensity factors of semi-elliptical surface cracks in pressure vessels by global–local finite element methodology). Engineering Fracture Mechanics 72, 1299–1312.

Duarte, C.A., Babuška, I., Oden, J.T., 2000. Generalized finite element methods for three-dimensional structural mechanics problems. Computers and Structures 77 (2), 215–232.

Duarte, C.A., Kim, D.J., 2008. Analysis and applications of a generalized finite element method with global–local enrichment functions. Computer Methods in Applied Mechanics and Engineering 197 (6–8), 487–504.

Duarte, C.A., Kim, D.-J., Babuska, I., 2007a (Chapter: a global–local approach for the construction of enrichment functions for the generalized fem and its application to three-dimensional cracks). In: Leitao, V.M.A., Alves, C.J.S., Duarte, C.A. (Eds.), Advances in Meshfree Techniques, Computational Methods in Applied Sciences, vol. 5. Springer, The Netherlands.

Duarte, C.A., Oden, J.T., 1996. An h-p adaptive method using clouds. Computer Methods in Applied Mechanics and Engineering 139 (1–4), 237–262.

Duarte, C.A., Reno, L.G., Simone, A., 2007b. High-order generalized FEM for through-the-thickness branched cracks. International Journal for Numerical Methods in Engineering 72 (3), 325–351.

Evangelista Jr., F., Roesler, J.R., 2009. Top–down cracking predictions for airfield rigid pavements. Transportation Research Record 2095, 13–23.

Evangelista Jr., F., Roesler, J.R., 2010. Alternative fatigue cracking modes for airfield rigid pavement design: 2D and 3D finite element analyses. COE Report No. 32, 108 pp., Center of Excellence for Airport Technology (CEAT), Department of Civil and Environmental Engineering, University of Illinois at Urbana-Champaign, Urbana, IL, USA.

Fish, J., 1992. The s-version of the finite element method. Computers and Structures 43, 539–547.

Garzon, J., Duarte, C.A., Buttlar, W.G., 2010. Analysis of reflective cracks in airfield pavements using a 3-D generalized finite element method. Road Materials and Pavement Design 11 (2), 459–477.

Guidault, P.-A., Allix, O., Champaney, L., Cornuault, C., 2008. A multiscale extended finite element method for crack propagation. Computer Methods in Applied Mechanics and Engineering 197, 381–399.

Ghosh, S., Lee, K., Raghavan, P.A., 2001. Multi-level computational model for multi-scale analysis in composite and porous materials. International Journal of Solids and Structures 38, 2335–2385.

Gupta, V., Kim, D.-J., Duarte, C.A., in press. Analysis and improvements of global-local enrichments for the generalized finite element method. Computer Methods in Applied Mechanics and Engineering. DOI: http://dx.doi.org/10.1016/j.cma.2012.06.021.

Heath, A.C., Roesler, J.R., 2000. Top–down cracking of rigid pavements constructed with fast-setting hydraulic cement concrete. Transportation Research Record 1712, 3–12.

Hussain, M.A., Pu, S.U., Underwood, J., 1974. Strain energy release rate for a crack under combined mode I and II. ASTM STP 560, 2–28.

Kim, D.J., Duarte, C.A., Pereira, J.P., 2008. Analysis of interacting cracks using the generalized finite element method with global–local enrichment functions. Journal of Applied Mechanics 75, 051107.

Kim, D.J., Duarte, C.A., Sobh, N.A., 2011. Parallel simulations of three-dimensional cracks using the generalized finite element method. Computational Mechanics 47 (3), 265–282.

Kim, D.J., Pereira, J.P., Duarte, C.A., 2010. Analysis of three-dimensional fracture mechanics problems: a two-scale approach using coarse-generalized fem meshes. International Journal for Numerical Methods in Engineering 81 (3), 335–365.

Lancaster, P., Salkauskas, K., 1981. Surfaces generated by moving least squares methods. Mathematics of Computation 37 (155), 141–158.

Lancaster, P., Salkauskas, K., 1986. Curve and Surface Fitting, An Introduction. Academic Press, San Diego.

Loehnert, S., Belytschko, T., 2007. A multiscale projection method for macro/microcrack simulations. International Journal for Numerical Methods in Engineering 71 (12), 1466–1482.

Liu, W.K., McVeigh, C., 2008. Predictive multiscale theory for design of heterogenous materials. Computational Mechanics 42 (2), 147–170.

McVeigh, C., Vernerey, F., Liu, W.K., Brinson, L.C., 2006. Multiresolution analysis for material design. Computer Methods in Applied Mechanics and Engineering 195 (37–40), 5053–5076.

Noor, A.K., 1986. Global–local methodologies and their applications to nonlinear analysis. Finite Elements in Analysis and Design 2, 333–346.

O'Hara, P., Duarte, C.A., Eason, T., Kim, D.-J., 2009. Generalized finite element analysis of three-dimensional heat transfer problems exhibiting sharp thermal gradients. Computer Methods in Applied Mechanics and Engineering 198 (21–26), 1857–1871.

Oden, J.T., Duarte, C.A., Zienkiewicz, O.C., 1998. A new cloud-based Hp finite element method. Computer Methods in Applied Mechanics and Engineering 153 (1–2), 117–126.

Pereira, J.P., 2010. Generalized finite element methods for three-dimensional crack growth simulations. Ph.D. Dissertation. University of Illinois at Urbana-Champaign, USA.

Pereira, J.P., Duarte, C.A., 2006. The contour integral method for loaded cracks. Communications in Numerical Methods in Engineering 22 (5), 421–432.

Pereira, J.P., Duarte, C.A., Guoy, D., Jiao, X., 2009. Hp-generalized FEM and crack surface representation for non-planar 3-D cracks. International Journal for Numerical Methods in Engineering 77 (5), 601–633.

Pereira, J.P., Duarte, C.A., Jiao, X., 2010. Three-dimensional crack growth with Hp-generalized finite element and face offsetting methods RID B-1753-2008. Computational Mechanics 46 (3), 431–453.

Rao, S., Roesler, J.R., 2005. Characterizing effective built-in curling from concrete pavement field measurements. Journal of Transportation Engineering 131 (4), 320–327.

Szabó, B., Babuška, I., 1991 (Finite Element Analysis). Wiley-Interscience.

Tanaka, K., 1974 (Fatigue propagation from a crack inclined to the cyclic tensile axis). Engineering Fracture Mechanics 6, 493–507.